Materials Research Bulletin 60 (2014) e222–e231

Contents lists available at ScienceDirect

Materials Research Bulletin

journal homepage: www.elsevier.com/locate/matresbu

Structural and vibrational investigations of Nb-doped TiO_2 thin films

E. Uyanga [a,d,*], A. Gibaud [b], P. Daniel [b], D. Sangaa [a], G. Sevjidsuren [a], P. Altantsog [a], T. Beuvier [b], Chih Hao Lee [c], A.M. Balagurov [d]

[a] Institute of Physics and Technology, Mongolian Academy of Sciences, Enkhtaivan Avenue 54B, Ulaanbaatar 13330, Mongolia
[b] LUNAM Université, Université du Maine, CNRS UMR 6283, Institut des molécules et matériaux et du Mans–IMMM, Avenue Olivier Messiaen, Le Mans 72085 Cedex 9, France
[c] Department of Engineering and System Science, National Tsing Hua University, Hsinchu 30013, Taiwan
[d] Frank Laboratory of Neutron Physics, JINR, Dubna 141980, Russia

ARTICLE INFO

Article history:
Received 13 January 2014
Received in revised form 17 August 2014
Accepted 25 August 2014
Available online 27 August 2014

Keywords:
Oxides
Sol–gel chemistry
Raman spectroscopy
X-ray diffraction
Crystal structure
Defects

ABSTRACT

Acid-catalyzed sol–gel and spin-coating methods were used to prepare Nb-doped TiO_2 thin film. In this work, we studied the effect of niobium doping on the structure, surface, and absorption properties of TiO_2 by energy-dispersive X-ray spectroscopy (EDX), X-ray diffraction (XRD), X-ray reflectometry (XRR), X-ray photoelectron spectroscopy (XPS), Raman, and UV–vis absorption spectroscopy at various annealing temperatures. EDX spectra show that the Nb:Ti atomic ratios of the niobium-doped titania films are in good agreement with the nominal values (5 and 10%). XPS results suggest that charge compensation is achieved by the formation of Ti vacancies. Specific niobium phases are not observed, thus confirming that niobium is well incorporated into the titania crystal lattice. Thin films are amorphous at room temperature and the formation of anatase phase appeared at an annealing temperature close to 400 °C. The rutile phase was not observed even at 900 °C (XRD and Raman spectroscopy). Grain sizes and electron densities increased when the temperature was raised. Nb-doped films have higher electron densities and lower grain sizes due to niobium doping. Grain size inhibition can be explained by lattice stress induced by the incorporation of larger Nb^{5+} ions into the lattice. The band gap energy of indirect transition of the TiO_2 thin films was calculated to be about 3.03 eV. After niobium doping, it decreased to 2.40 eV.
© 2014 Elsevier Ltd. All rights reserved.

1. Introduction

TiO_2 is by far one of the most studied compounds in the world because its semiconductor properties combined with an outstanding resistance to corrosion in aqueous environments make it the perfect material for photovoltaic, photocatalytic, and fuel cell applications [1–3]. It is presently considered as an alternative catalytic support for cathode catalysts in polymer electrolyte membrane fuel cells (PEMFCs) because it is stable in a fuel cell operation atmosphere, commercially available at low cost, and stable in water and can be synthesized with a controlled size and structure [4–7]. However, its low electrical conductivity presents a strong drawback for its use in fuel cells. Therefore, it is important to explore possibilities for synthesizing TiO_2 with better electrical conductivity [8–10]. At room temperature, TiO_2 occurs in three commonly known polymorphic crystal forms: anatase, rutile, and brookite. Among these three phases, rutile is the most stable one thermally. When heated, anatase (at ~550 °C) and brookite (at ~750 °C) undergo a structural phase transition above 600 °C and are converted into rutile. At high temperature, the anatase phase of titania is usually stabilized by cation addition. It is desirable for fuel cell catalysts due to its better catalytic activity for oxidizing organic compounds compared to the rutile and brookite structures. However, the indirect allowed band gap of anatase is slightly larger than that of rutile: they are 3.2 and 3.02 eV, respectively. In order to decrease this gap, extrinsic doping of anions or cations is performed. For instance, nitrogen-doped TiO_2 is known to have a reduced band gap of 2.6 eV because N p states contribute to the band-gap narrowing by mixing with O 2p states [11]. In such a case, N-doped TiO_2 has a photocatalytic activity in the visible range of the solar spectrum [12]. Doping by metallic ions has also been considered to improve the lifetime of excitons at the surface of TiO_2 nanoparticles. In the case of Nb doping, it has been shown that Nb-doped anatase exhibits an improved electrical conductivity, making such a compound promising for use as a transparent

* Corresponding author at: Frank Laboratory of Neutron Physics, JINR, Joliot-Curie str., Dubna 6141980, Moscow, Russia.
E-mail address: uyanga.enkhnaran@gmail.com (E. Uyanga).

http://dx.doi.org/10.1016/j.materresbull.2014.08.035
0025-5408/© 2014 Elsevier Ltd. All rights reserved.

conducting oxide. By doping it is indeed possible to add localized states in the gap so that the Fermi level shifts in energy without changing the band edges [13,14].

The incorporation of Nb into titania yields changes in the electronic structure that have been extensively discussed in the literature. In particular, Nb^{5+} ions embedded into the anatase titania crystalline structure hinder its phase transformation to rutile and inhibit grain growth. To compensate the excessive charge of Nb^{5+} in substitution for Ti^{4+}, two mechanisms have been proposed. A first possibility is offered if one Ti^{4+} cation vacancy is created for every four Nb^{5+} (Eq. (1)). Alternatively, reducing Ti^{4+} to Ti^{3+} for every Nb^{5+} incorporated is also possible (Eq. (2)) [15–18].

$$\frac{1}{2}Nb_2O_5 + Ti_{ti}^{x} \rightarrow Nb_{Ti}^{\cdot} + \frac{1}{4}V_{Ti}^{''''} + TiO_2 + \frac{1}{4}O_2 \quad (1)$$

$$\frac{1}{2}Nb_2O_5 + Ti_{ti}^{x} \rightarrow Nb_{Ti}^{\cdot} + Ti_{Ti}^{'} + \frac{5}{4}O_2 \quad (2)$$

Another important consequence of the multivalent cation doping is an increase in the electrical conductivity of TiO_2, which is low at ambient temperature.

In this paper we report the preparation of TiO_2 thin films by using the acid-catalyzed sol–gel method and the spin-coating technique to deposit the films on silicon substrates. The effect of niobium doping on the structure, surface, and absorption properties of TiO_2 was characterized by several techniques, including *in situ* X-ray diffraction (XRD), X-ray reflectivity (XRR), X-ray photoemission spectroscopy (XPS), energy dispersive X-ray analysis (EDX), and UV–vis spectroscopy. The main attention was paid to the evolution of a TiO_2 structure with the niobium doping under various annealing conditions.

2. Experimental

2.1. Sample preparation

2.1.1. Preparation of $Nb_xTi_{1-x}O_2$ support

In this work we chose two different percentages of niobium content, 10 and 5% ($x = 0.1$ and $x = 0.05$, respectively). TiO_2 was prepared by an acid-catalyzed sol–gel method in a non-aqueous medium. Typically, 1 g of titanium isopropoxide (Acros, 98%) and 1.24 g of hydrochloric acid (Aldrich, 37%) were added to 10 g of isopropanol (Acros, 99.6%) and stirred for 10 min. Subsequently, an appropriate amount of niobium (V) ethoxide (Aldrich, 99.95%) was added to the solution to achieve Nb concentrations of 5 and 10% relative to Ti.

2.1.2. Preparation of thin films

Four to five drops of TiO_2- and Nb-doped TiO_2 solutions were spun (using a SussMicroTec RC8 spin coater) onto silica-coated silicon substrates (2.5 cm × 2.5 cm) at a rate of 4000 rpm for 60 s.

2.2. Characterization methods

The *in situ* XRR and XRD measurements were carried out using Cu Kα radiation (wavelength of 1.54 Å) on a PANalytical Empyrean system working at 40 kV and 30 mA. The white beam from a copper anode was monochromatized and collimated by reflection on a mirror so as to obtain a parallel beam. The full width at half maximum of the direct beam was typically 0.06° with peak intensity of the order of 50×10^6 cts/s. The size of the incident beam was about 10 mm × 100 μm.

The angular resolution of the XRR instrument was 0.008°. Data fitting was performed with a Matlab-based Reflex15 simulation Matlab routine with the Matrix technique. XRD data were collected with a step size 0.08° and a count time 5 s per step. The structure was refined by the Rietveld method using the material analysis using diffraction (MAUD) package with the EXPGUI graphical user interface.

The samples were mounted in a DHS1100 temperature attachment from Anton-Paar GmbH. The annealing temperatures ranged from 25 to 900 °C in steps of 25 °C. The thermal treatment applied to all the samples was a heating ramp of 60 °C/min and the holding temperature for 1 h, with the whole process being carried out under atmospheric air.

The UV–vis spectra of the thin films were recorded in the reflectance mode on an Ocean Optics HR4000 spectrometer. The scan range was from 200 to 1100 nm with a 0.23 nm interval, and the averaging time at each point was 7 s. For the elemental analysis of the Nb-doped TiO_2 thin film, EDX analysis was performed using a JSM-66510LV (JEOL) instrument. Raman scatterings were measured using a Jobin Yvon T64000 spectrometer coupled to a

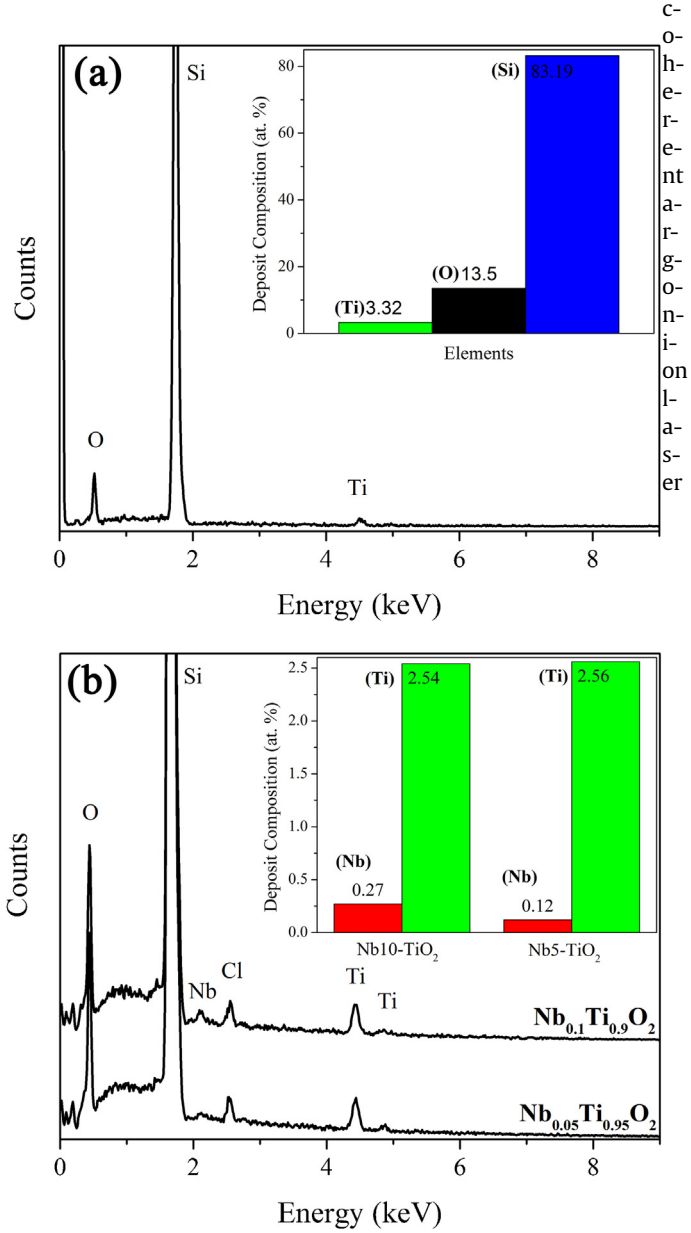

Fig. 1. EDX analysis results of (a) TiO_2- and (b) Nb-doped TiO_2 deposition on silicon substrate. For TiO_2 film the oxygen content is composed of oxygen in the film itself and silica with which Si is coated. For Nb-doped TiO_2 films, the actual ratios are quite similar to the nominal values: 21.3 and 19 for $x = 0.05$; 9.4 and 9 for $x = 0.1$.

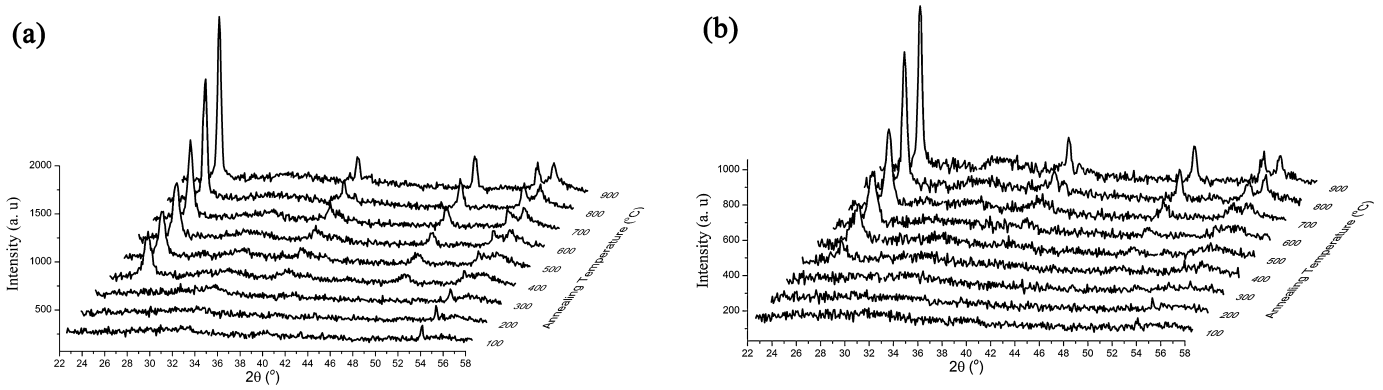

Fig. 2. *In situ* XRD patterns of TiO_2(a) and $Nb_{0.1}Ti_{0.9}O_2$ (b) at various annealing temperatures in the 100–900 °C range. The initial state is amorphous for both films; the diffraction peaks of anatase phase appear at about 375 °C.

with the 514.5 nm polarized green line selected. High-temperature measurements were carried out using a Linkam TS1500 heating stage with temperature range of 25–900 °C. The measurements were done under a microscope (Olympus BX 40) with a magnification of 50×. The scan range was 100–2300 cm^{-1}. Each measurement was repeated twice and the duration of acquisition was 60 s.

Surface compositions and the composition distribution along the depth of the thin films were characterized by XPS at the National Synchrotron Radiation Research Center in Taiwan. The binding energies were calibrated using the Au $4f_{7/2}$ feature at 84 eV as a standard. The XPS etching area was 5 mm × 5 mm. The sensitivity factors were Ti 2p = 1.8, O 1s = 0.66, and Nb 3d = 2.4. The atomic concentration of each element was calculated by determining the relevant integral peak intensity. The Shirley method [19] of background removal was used in the least squares fitting.

3. Results and discussion

3.1. EDX analysis

Fig. 1 shows the results of the EDX analysis of the content elements of thin films. In particular, attention was focused on the Nb and Ti contents. Bar graphs in the inset of Fig. 1 indicate the Si, O, Ti, and Nb elemental percentages of the substances. In the pure TiO_2, we observed the presence of 83.19 at.% Si, 13.5 at.% Ti, and 3.32 at.% O (Fig. 1(a)). The presence of silicon is attributed to the substrate while the oxygen signal comes from both TiO_2 and SiO_2 as the silicon substrate was silica coated.

With regard to the $Nb_xTi_{1-x}O_2$ films, in the EDX spectra there are signals of Si, O, Ti, and Nb and some Cl impurity. For $x = 0.05$ we find 0.12 at.% of Nb and 2.56 at.% of Ti with a Ti:Nb ratio equal to 21.3 instead of a nominal value of 19. For $x = 0.1$, we find 0.27 at.% of Nb and 2.54 at.% of Ti with a Ti:Nb ratio equal to 9.4 instead of a nominal value of 9. Thus the actual ratios are quite similar to the nominal values.

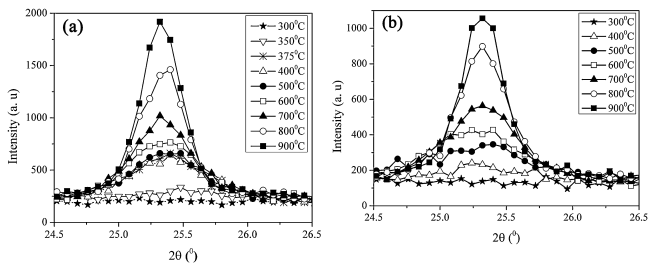

Fig. 3. *In situ* XRD profiles of the anatase (1 0 1) peak of (a) TiO_2 and (b) $Nb_{0.1}Ti_{0.9}O_2$ thin films. The crystal (anatase) phase appears above 350 °C.

3.2. XRD characterization

XRD measurements confirm that the fabricated films are amorphous. To promote the crystallization, films were annealed step by step up to 900 °C. The crystallization was monitored *in situ* during the annealing process. The evolution of the X-ray diffraction patterns for the TiO_2- and Nb- ($x = 0.1$) doped TiO_2 thin films is shown in Fig. 2. Scattering patterns were collected at a grazing incidence of 0.3° to take advantage of the finite thickness of the film. We observe that the onset of the phase transformation for both films occurs between 350 and 375 °C, where the anatase peaks appear. The peak intensities increase further when the temperature is raised to 900 °C. We observe that in our thin films the rutile phase is not formed (at ~550 °C), which can be attributed to the preparation procedure. The same feature was reported in [20], which states that the phase transformation from anatase to rutile occurs at 1000 °C when HCl is used as a catalyst in sol–gel formation. It is also important to notice that the temperature at which the phase transformation occurs is strongly dependent on the temperature ramp used. Steady-state measurements performed as a function of time by Kirsch et al. [21] show that for

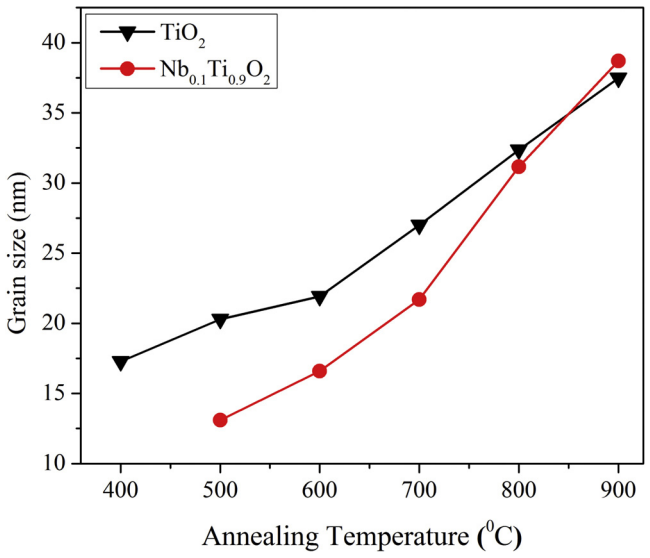

Fig. 4. Evolution of the grain sizes at various annealing temperatures. Up to 800 °C, the grain size of $Nb_{0.1}Ti_{0.9}O_2$ is smaller than for pure TiO_2 because doped Nb hinders the growth of the TiO_2 grains.

Table 1
Particle sizes of anatase phase at various temperatures.

Temperature (°C)		400	500	600	700	800	900
Particle size (nm)	TiO_2	17.28	20.29	21.92	27	32.36	37.48
	$Nb_{0.1}Ti_{0.9}O_2$	–	13.1	16.59	21.68	31.15	38.71

mesoporous titania the kinetics of formation of anatase can be described by an Avrami law.

The evolution of the anatase (1 0 1) diffraction peak is shown in Fig. 3. The initial amorphous state is crystallized as an anatase phase above 350 °C. Analysis of diffraction intensities undoubtedly shows that Ti is substituted by Nb in the doped films. This substitution is expected to induce slight strain in the titania lattice that may prevent the growth of large TiO_2 crystallites [22].

XRD was used to evaluate the average grain size of Nb-doped TiO_2 support by the Scherer equation. Fig. 4 shows the grain size evolution for TiO_2- and Nb- ($x = 0.1$) doped TiO_2 thin films in the range of 100–900 °C. Up to 800 °C, the grain size of $Nb_{0.1}Ti_{0.9}O_2$ is smaller than that of pure TiO_2. This is consistent with the fact that Nb hinders the growth of the TiO_2 grains. Above 800 °C, the grain size of $Nb_{0.1}Ti_{0.9}O_2$ increased rapidly. This may be the possible signature that Nb atoms become segregated from TiO_2 when the temperature becomes high enough. The average grain sizes at various temperatures are presented in Table 1.

3.3. XPS analysis

The chemical composition and surface oxidation states of Nb-doped thin films were analyzed by X-ray photoelectron spectroscopy. Fig. 5 shows typical XPS spectra for amorphous TiO_2- and Nb-doped TiO_2 films. One can clearly recognize the Ti 2p region located between 454 and 468 eV, the O 1s region located between

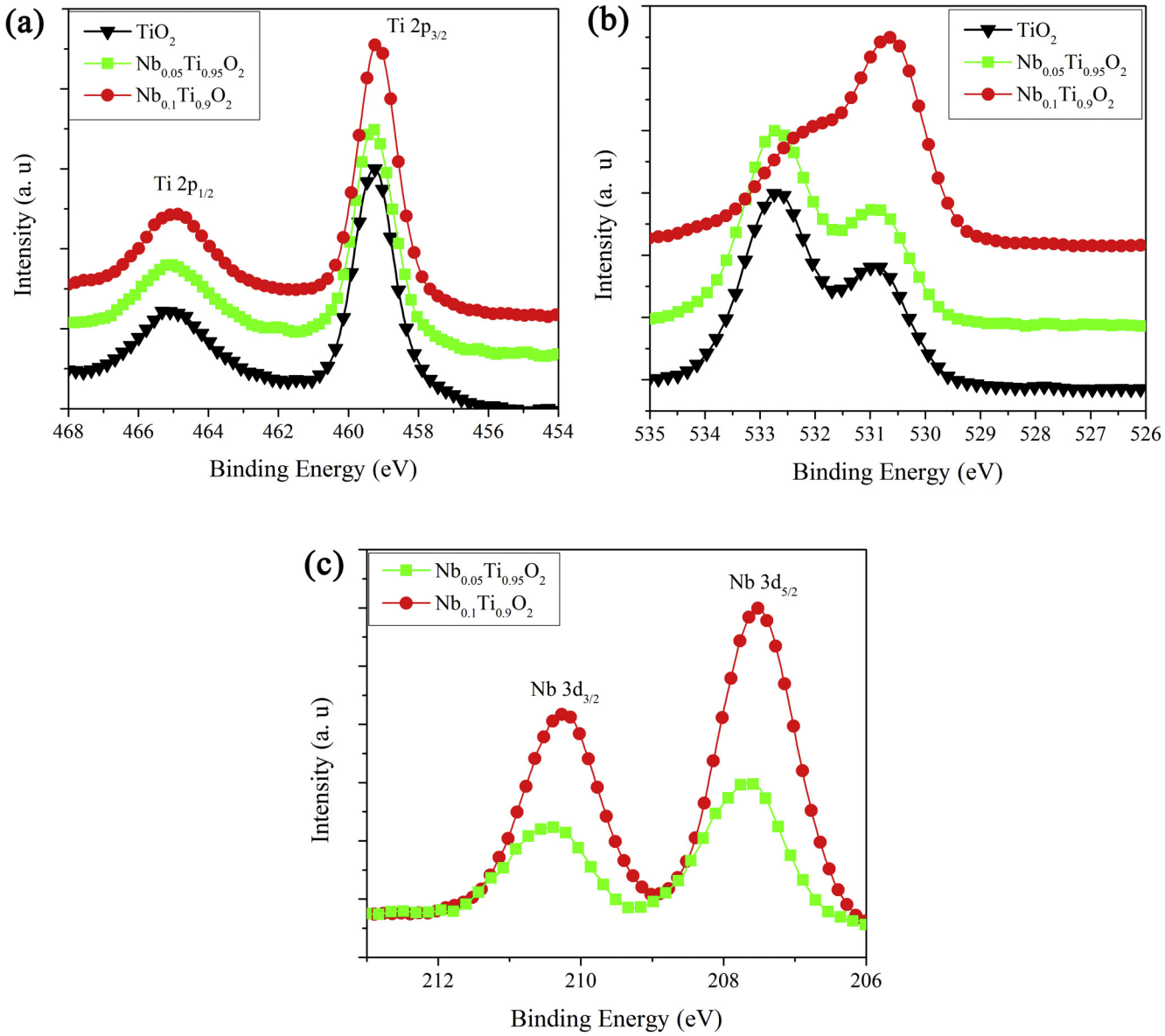

Fig. 5. XPS spectra of (a) Ti 2p, (b) O 1s, and (c) Nb 3d of prepared thin films. The intensity in the XPS spectra was normalized by the base line. The films indicate that Nb exists mainly as Nb^{5+} while Ti exists mainly as Ti^{4+}.

Table 2
XPS data fitting results.

Samples	Experimental (at.%)		
	Ti	O	Nb
TiO_2	19.6	80.4	–
$Nb_{0.05}$ $Ti_{0.95}O_2$	18.2	79.7	2.1
$Nb_{0.1}$ $Ti_{0.9}O_2$	22.6	72.3	5.1

527 and 535 eV, and the Nb 3d region between 206 and 213 eV. It must be noted that in all spectra a peak at around 281.5 eV was found (not shown in this work), corresponding to carbon impurities probably arising from the background of the XPS test or the residual precursors. The binding energy of all the spectra was calibrated to the C 1s photoemission. Shirley-type background subtraction was applied to the photoemission lines, which were fitted using a combination of Gaussian–Lorentzian line shapes (CasaXPS).

Fig. 5(a) shows two broad peaks of Ti 2p from undoped and Nb-doped TiO_2. The binding energies close to 459 and 465 eV correspond to $2p_{3/2}$ and $2p_{1/2}$ of Ti^{+4}, respectively [23–27]. Peaks of doped TiO_2 exhibit a small shift compared to those of pure TiO_2, due to substitution of the Nb^{+5} in the TiO_2 lattice and the possible formation of Nb—O—Ti bonds in the film. Compared to Nb 5 mol% (459.1 eV), peaks of Nb 10 mol% doped titania (459.3 eV) shifted to lower binding energy.

Fig. 5(b) shows the O 1s core-level spectra of pure and doped TiO_2. The chemical shift and peak intensity of O 1s are similar in pure and Nb 5 mol% doped TiO_2 film. The peak at 530.9 eV for the pure sample is due to O^{2-} ions in the TiO_2 lattice (Ti—O—Ti), whereas the peak at 532.7 eV can be attributed to the surface hydroxyl groups (Ti—OH) on the titania [28]. The main contribution is attributed to OH groups belonging to hydroxyl groups or adsorbed H_2O and the minor contribution to the remnant Ti—OH bonds formed during sol–gel synthesis.

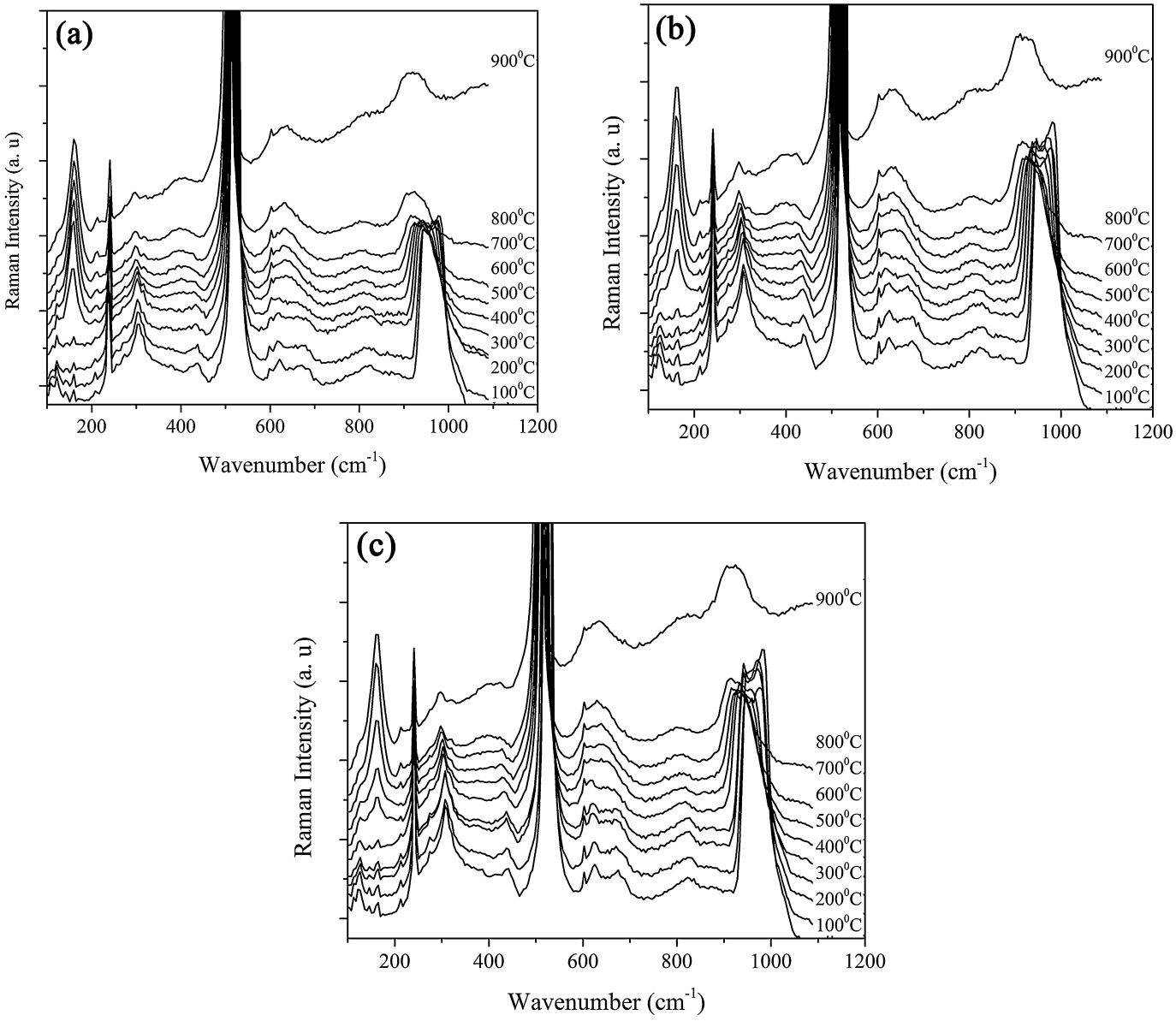

Fig. 6. Raman spectra of (a) TiO_2, (b) $Nb_{0.05}Ti_{0.95}O_2$, and (c) $Nb_{0.1}Ti_{0.9}O_2$ thin films at various annealing temperatures. The initial state is amorphous for films; this amorphous phase crystallizes into the anatase structure above 400 °C (E_g peak at 159 cm^{-1}).

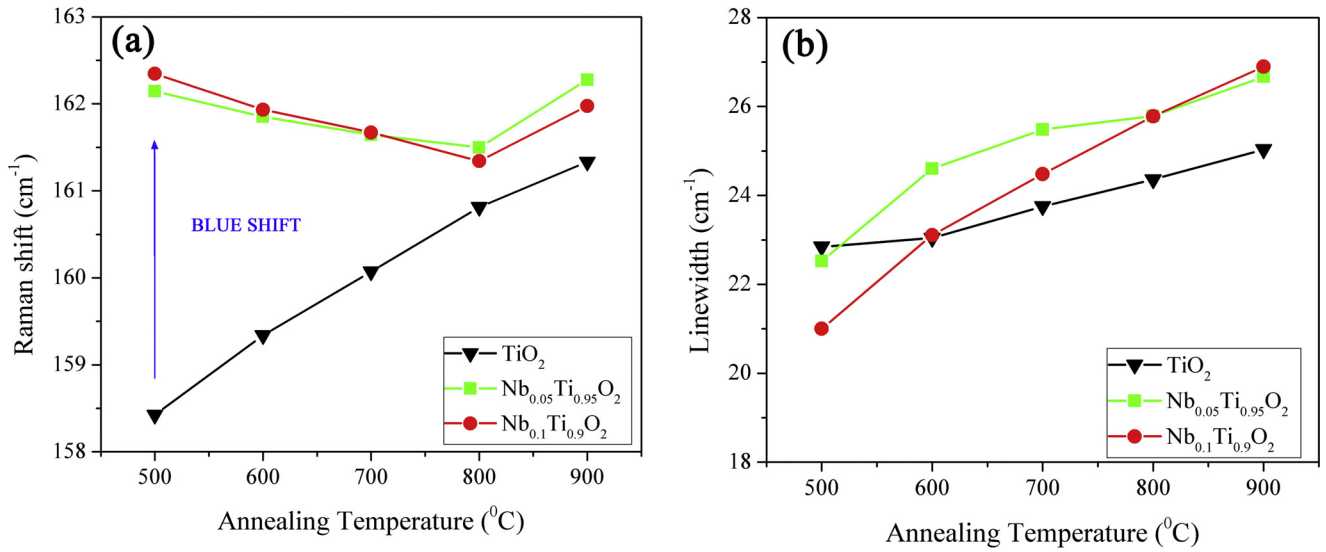

Fig. 7. Evolution of the (a) Raman shift and (b) linewidth of E_g mode versus annealing temperature. The blue shifts of the low frequency E_g modes for Nb-doped thin films appeared due to the incorporation of substitutional niobium dopants.

The O 1s XPS spectra show dramatic changes with a major contribution from TiO_2 bonds, as can be seen in Fig. 5(b). Because the O 1s feature in metal oxides is strongly affected by the local electronic structure of metal–oxygen bonds, the spectral change is an indication that the increased niobium content in $Nb_{0.1}Ti_{0.9}O_2$ induced a perturbation in the local electronic structure.

The XPS peak intensity of $Nb_{0.05}Ti_{0.95}O_2$ film is weaker than that of $Nb_{0.1}Ti_{0.9}O_2$ (Fig. 5(c)) due to the lower doping level. The binding energies from 207.5 to 207.7 eV and from 210.2 to 210.4 eV should be assigned to 3d 5/2 and 3d 3/2 of Nb^{5+}, respectively. The chemical valence of doped Nb in the films is +5. The Nb^{5+} may be induced by the oxygen vacancies since no Nb_2O_5 phase was observed from the XRD measurement. This means that charge compensation is achieved by the formation of Ti vacancies according to Eq. (1).

The atomic percentages of the elements Ti, Nb, and O at the top surface of the Ti—Nb—O oxide films are shown in Table 2.

3.4. Raman measurements

We can observe well-defined Raman bands between 100 and 1200 cm^{-1} that are characteristic of the anatase phase. Fig. 6 shows *in situ* Raman spectra of TiO_2 thin films. The samples were investigated in the 50–900 °C temperature range. Raman spectra measured at temperatures between 100 and 300 °C confirm that the films are amorphous (we did not observe an E_g peak at 159 cm^{-1} until 400 °C). This amorphous phase crystallizes into the anatase structure above 400 °C. Bands of anatase appear at 159 cm^{-1} (E_g), 210 cm^{-1} (E_g), 393 cm^{-1} (E_{1g}), and 623 cm^{-1} (E_g) in all films. With increasing temperature, we observed the crystallization and growth of the anatase phase. Peaks at about 238, 292, 420, 598, and 960 cm^{-1} come from the silicon substrate. Raman experiments confirm that TiO_2 thin films do not exhibit any structural phase transition from anatase to rutile, in agreement with our X-ray analysis. Additionally, bands of niobia phases are not observed, indicating that there is no phase separation or formation of NbO_x at the surface of TiO_2 particles.

The E_g mode is strongly dependent on the annealing treatment and arises from the extension vibration of the anatase structure. The evolution of the E_g Raman mode (the peak position, linewidth, and shape) can be attributed to the phonon confinement, strain, non-stoichiometric defects, and anharmonic effects of lattice potential due to the annealing temperature [29,30]. The symmetric shape of E_g modes up to 800 °C indicates a strong anharmonic effect, while at 900 °C their more asymmetric broadening shows that a pronounced phonon confinement effect is dominant.

The frequency and linewidth of the E_g modes (strongest band) for TiO_2- and Nb-doped TiO_2 thin films annealed at various temperatures are shown in Fig. 7. The frequency and linewidth are obtained by fitting the data to Lorentzian and Gaussian line shapes. Comparing the Raman spectra for the three thin films, we observe a blue shift of the low frequency E_g modes for Nb-doped thin films. This is attributed to the incorporation of substitutional niobium dopants.

With increasing annealing temperature, the intensity of the E_g mode of undoped TiO_2 increases and is accompanied by a slight shift to a higher wavenumber (blue shift) and linewidth broadening. These results suggest that the size effect has a greater influence on the E_g mode than the anharmonic effect. The particle sizes of undoped TiO_2 grow with the upshift of the E_g mode frequency during annealing.

The red shift and broadening of the E_g mode of Nb-doped TiO_2 during annealing clearly point to the fact that anharmonic effects have a greater influence on the frequency and line-width up to 800 °C than size effects. At 900 °C, size effects become dominant over anharmonic effects in E_g Raman mode. This effect may be explained by the fact that Nb atoms segregate from the TiO_2 lattice.

3.5. XRR characterization

Fig. 8 shows the X-ray reflectivity curves of annealed TiO_2 and Nb-doped ($x = 0.05, 0.1$) TiO_2 films at various temperatures ranging from 50 to 700 °C. The data are plotted on a logarithmic scale so that the intensities can be clearly observed. The intensity oscillation of the XRR curves originated from the film thickness.

XRR curves exhibit two very clear temperature-dependent features at the same time:

- Kiessig fringes (oscillations) which are characteristic of the finite thickness of the film. Their amplitudes are related to the contrast of electron density between the film and the underlying substrate
- A critical q-value, q_c, which is connected with the total reflection cut-off.

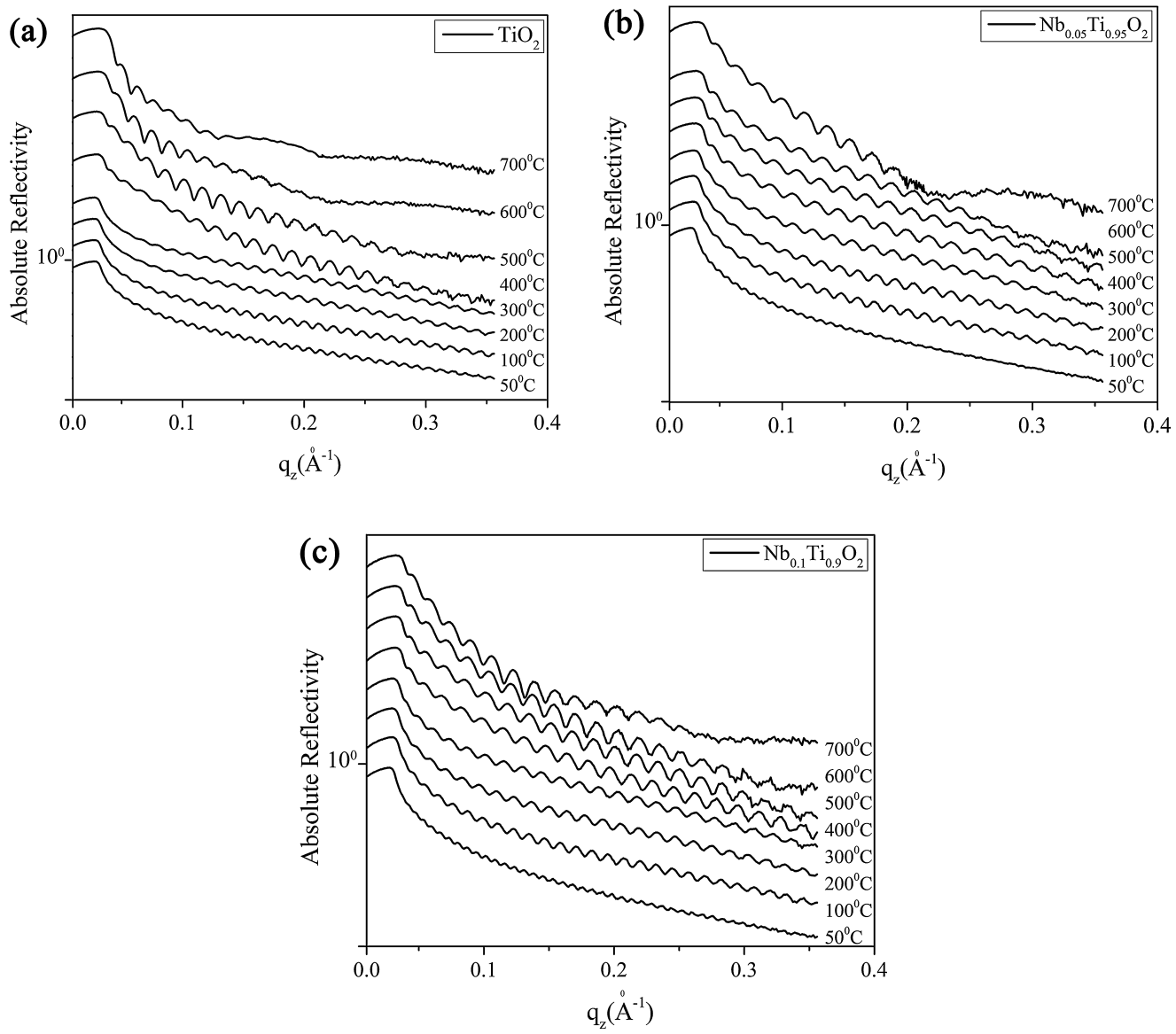

Fig. 8. XRR curves of (a) TiO_2, (b) $Nb_{0.05}Ti_{0.95}O_2$, and (c) $Nb_{0.1}Ti_{0.9}O_2$ thin films at various annealing temperatures. The evolution of the amplitude of Kiessig fringes shows the densification of the films. The Kiessig fringes are well contrasted at 400 and 500 °C. Below 400 °C, the fringes, although weak, persist up to quite large values of q, thus showing that the surface of the film is quite smooth.

These two parameters are clearly temperature-dependent. As shown in Fig. 8, the amplitude of Kiessig fringes is quite weak at 50 °C. It increases slightly until a temperature of 400 °C is reached. After that, it becomes more pronounced when the temperature is raised. This observation is concomitant with the increase of the critical q_c of the film at a low q wave vector transfer [31]. Both observations are consistent with the densification of the films. The Kiessig fringes are well contrasted at 400 and 500 °C. Below 400 °C, the fringes, although weak, persist up to quite large values of q, thus showing that the surface of the film is quite smooth. This is confirmed by the X-ray reflectivity curve-fitting results. At 600 and 700 °C, the amplitude of the Kiessig fringes dropped due to an increase of the surface roughness (Fig. 8). Further increases in temperature induce the appearance of a layer in the film and some important surface roughness (not shown here).

The electron density and thickness obtained by fitting reflectivity data for the three films are plotted in Fig. 9. The film thickness decreases rapidly when the temperature is raised to 300 °C. In this temperature range, the thickness decreases because the films are mainly losing water molecules and isopropanol molecules. Between 400 and 700 °C, the thickness is almost constant during the transformation of the amorphous phase into the anatase one. Above 700 °C, the change is mainly due to the sintering of the TiO_2 film.

Below 600 °C, the electron density of Nb-doped TiO_2 films is higher than that of pure TiO_2 thin film. In particular the $x = 0.1$ niobium-doped film displays the highest electron density. Between 300 and 400 °C, the electron density increases steadily as a consequence of the transformation from the amorphous to the anatase phase. This transformation is the result of the densification of the gel phase into a crystalline phase by condensation of an OH pendant group at the surface of TiO_2. This is accompanied by a decrease of the film thickness due to the sintering of the film which is visible over the entire range of temperatures. Surprisingly it can be seen that at elevated temperatures ($T > 700$ °C), the electron density of TiO_2 becomes higher than that of the Nb-doped TiO_2. This might be related to the segregation of Nb atoms from the TiO_2 lattice.

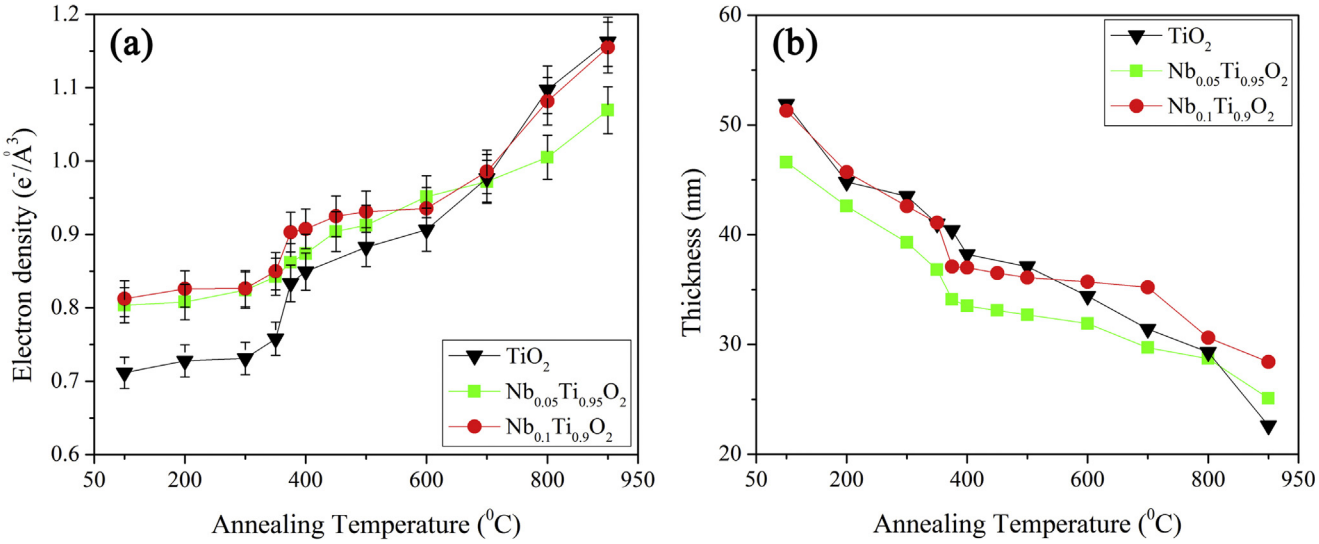

Fig. 9. Evolution of (a) electron density and (b) thickness versus annealing temperature. The step-like increase in electron density and slightly smoother decrease of the film thickness are fully consistent with the fact that below 300 °C the TiO_2 gel is losing water molecules as a result of water evaporation and syneresis.

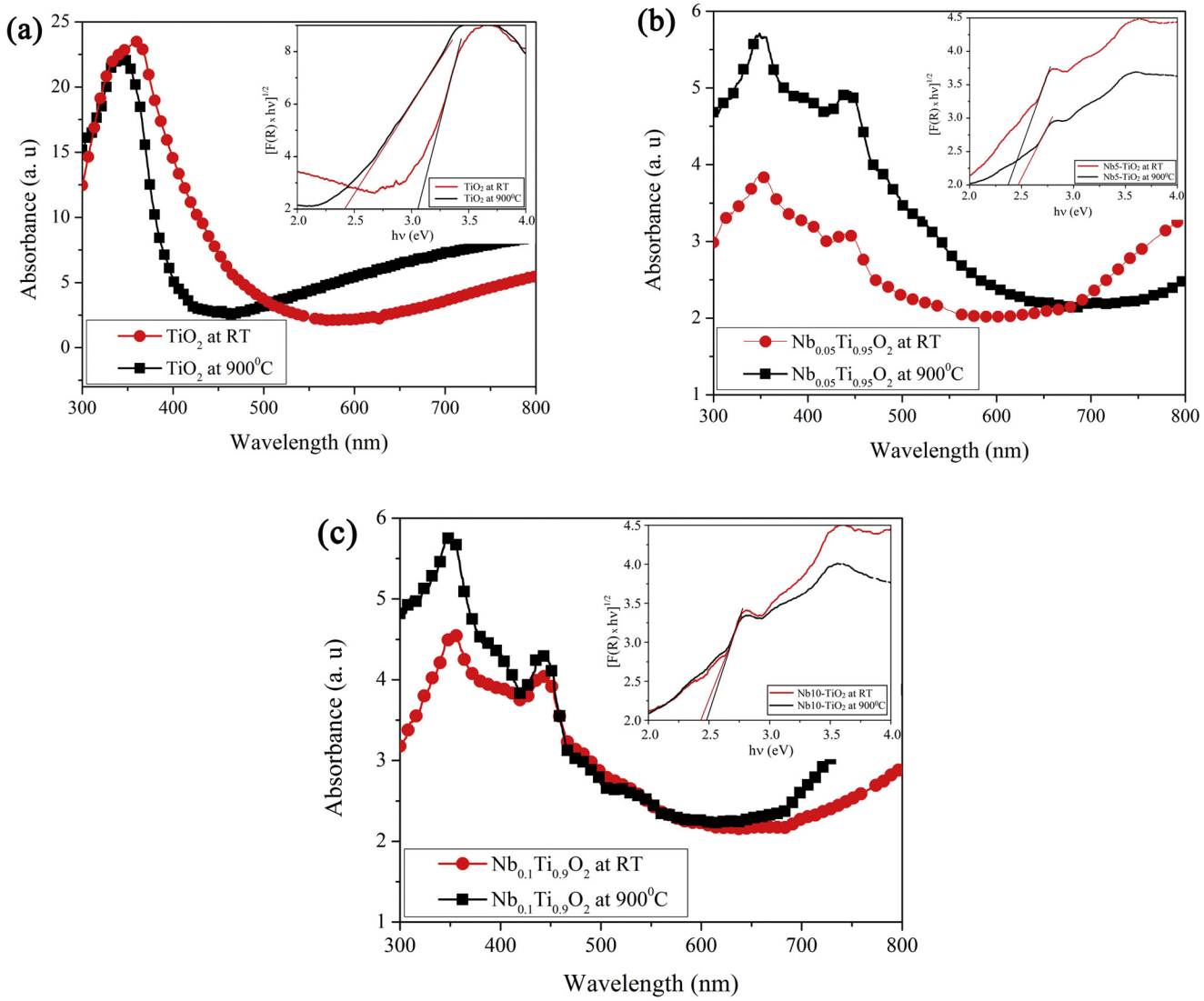

Fig. 10. UV–vis absorbance spectra of (a) TiO_2, (b) Nb 5 mol%, and (c) Nb 10 mol% doped TiO_2. (Inset graph: energy band gap calculation by extrapolation). The band gaps for all films are about the same and equal to 2.40 eV before annealing. After annealing at 900 °C, the gaps of pure and Nb doped TiO_2 changed to about 3.03 and 2.4 eV, respectively.

Table 3
Band gap calculation results.

	Samples	TiO_2	$Nb_{0.05}Ti_{0.95}O_2$	$Nb_{0.1}Ti_{0.9}O_2$
E_g (eV)	Before annealing	2.42	2.41	2.40
	After annealing	3.03	2.34	2.47

The step-like increase of the electron density and slightly smoother decrease of the film thickness are fully consistent with the fact that below 300 °C, the TiO_2 gel is losing water molecules as a result of water evaporation and syneresis. Around 400 °C, the steep change in electron density is a clear consequence of the phase transformation of amorphous titania into the anatase crystalline form. This aspect is confirmed by studying the X-ray pattern at a wide angle, as shown in Fig. 3.

3.6. UV–vis results

The UV absorption property of TiO_2 films is an important factor for photocatalysis. The UV spectra of TiO_2 and Nb- ($x = 0.05, 0.1$) doped TiO_2 films before ($T = 25$ °C) and after ($T = 900$ °C) calcinations are shown in Fig. 10. Spectra were recorded in reflectance mode and transformed mathematically into the normalized Kubelka–Munk function [32]. As we know, heteroatom doping in TiO_2 materials introduces defects such as oxygen vacancies, interstitial cation, and band gap variance. A single higher absorbance of TiO_2 film appeared at 340–358 nm, whereas Nb-doped TiO_2 film shows two optical absorption thresholds at 349–351 nm (ultraviolet region) and 440–443 nm (visible region). Broad absorption around 440 nm corresponds to niobium doping in the film. At 900 °C, the absorption spectra of the TiO_2 thin film show a blue shift in the absorption edge. Otherwise, the absorption spectra of the niobium 5 mol% doped TiO_2 shifted to higher absorbance (red shift) at 900 °C. The red shift is ascribed to the fact that Nb doping can narrow the band gap of the TiO_2. For niobium 10 mol% doped TiO_2, the shift in the band gap is less pronounced in the absorbance spectra.

The fundamental absorption, which corresponds to electron excitation from the valence band to the conduction band, can be used to determine the value of the indirect optical band gap. It has been reported that the band-gap electronic transition of anatase TiO_2 is indirect [33]. The incident photon energy $h\nu$ and absorption coefficient α are related through the well-known equation:

$$\alpha\eta\nu = C(h\nu - E_g)^{\frac{1}{2}} \quad (3)$$

where C is the proportionality constant and E_g is the optical band gap.

The indirect optical band gap values of thin films are calculated by extrapolating the straight line portion of the $(\alpha h\nu)^{1/2}$ versus $h\nu$ graph (Fig. 10). The value of the band gap is obtained by looking at the intercept with the $h\nu$ axis. It is found that the band gaps for all films are about the same and are equal to 2.40 eV before annealing. This value is smaller than 3.2 eV, which is reported for bulk TiO_2 anatase [34]. After annealing at 900 °C, the gap of pure TiO_2 increased to about 3.03 eV as a result of the phase transformation of the amorphous state into anatase. On the contrary, the band gap of Nb-doped films remained close to 2.4 eV after annealing (see Table 3).

4. Conclusions

In this work, the structural and dynamic properties of Nb-doped TiO_2 ($Nb_xTi_{1-x}O_2$) thin films under various temperatures in the range of 25–900 °C were studied. The films were prepared by the acid-catalyzed sol–gel method and the spin coating technique; the Nb contents were 5 and 10 mol% ($x = 0.05, 0.1$).

The EDX spectra show that the Nb:Ti atomic ratios of the niobium-doped titania films are quite similar to the nominal values. The XPS experimental results suggest that charge compensation of our thin films is achieved by the formation of Ti vacancies according to Eq. (1). When the niobium content reached 10 mol% it induced a perturbation in the local electronic structure.

No niobium phase was observed by XRD and Raman measurements, confirming that niobium is incorporated well into the titania crystal lattice. Thin films were amorphous at room temperature and the formation of anatase phase appeared at an annealing temperature close to 400 °C. Syneresis and the phase transformation of titania from the amorphous phase to the anatase phase were evidenced. No formation of rutile phases was observed until 900 °C. Generally, grain sizes and electron densities increased with increasing temperature (according to the XRR and XRD results). Nb-doped films have higher electron densities and lower grain sizes due to niobium doping. Grain size inhibition was explained by lattice stress induced by the larger Nb^{5+} ions incorporated into the lattice. Above 700 °C, we observed that the grain sizes of Nb-doped TiO_2 increased sharply, the electron densities were lower than in undoped TiO_2, and the Raman red shift changed to a blue shift. These phenomena could be explained by the effect of niobium segregation from the crystal lattice. However, we have not detected any niobium phase from XRD and Raman results at high temperatures.

The Nb-doped TiO_2 thin films exhibit a stronger absorption in the near UV and visible-light region and a red shift in the band-gap transition. Nb doping is incorporated into the crystal lattice and extends the absorbance spectra of TiO_2 into the visible region, which leads to a reduction in the band gap. After niobium doping, the band gap decreases to 2.40 eV. This value is very interesting for promoting photocatalytic degradation of pollutants in the visible range of the solar spectrum.

Consequently, our obtained experimental results show the evolution of the critical structure for a TiO_2 thin film as changes with Nb doping and annealing temperatures. These results could be very useful in the future for potential applications of structurally modified TiO_2 thin films.

Acknowledgements

The authors would like to thank the French Embassy in Mongolia and the Université du Maine (Ecole Doctorale 3MPL) for funding the visit of E. Uyanga to the Université of Maine (Le Mans, France). The help of Dr. Nicolas Errien with the UV–vis measurements is gratefully acknowledged.

References

[1] A.L. Linsebigler, G. Lu, J.T. Yates, Photocatalysis on TiO_2 surfaces: principles, mechanisms, and selected results, Chem. Rev. 95 (1995) 735–758.
[2] I.K. Konstantinou, T.A. Albanis, Photocatalytic transformation of pesticides in aqueous titanium dioxide suspensions using artificial and solar light: intermediates and degradation pathways, Appl. Catal. B. Environ. 42 (2003) 319–335.
[3] S.Y. Huang, P. Ganesan, B.N. Popov, Electrocatalytic activity and stability of niobium-doped titanium oxide supported platinum catalyst for polymer electrolyte membrane fuel cells, Appl. Catal. B 96 (2010) 224–231.
[4] S.L. Gojkovic, B.M. Babic, V.R. Radmilovic, N.V. Krstajic, Nb-doped TiO_2 as a support of Pt and Pt–Ru anode catalyst for PEMFCs, J. Electroanal. Chem. 639 (2010) 161–166.
[5] Z. Liu, J. Zhang, B. Han, J. Du, T. Mu, Y. Wang, Z. Sun, Solvothermal synthesis of mesoporous Eu_2O_3–TiO_2 composites, Micropor. Mesopor. Mater. 81 (2005) 169–174.
[6] B.L. Garcia, R. Fuentes, J.W. Weidner, Low-temperature synthesis of a PtRu/$Nb_{0.1}Ti_{0.9}O_2$ electrocatalyst for methanol oxidation, Electrochem. Solid State 10 (2007) 108–110.
[7] S. Sharma, B.G. Pollet, Support materials for PEMFC and DMFC electrocatalysts – a review, J. Power Source 208 (2012) 96–119.

[8] T.M. Breault, B.M. Bartlett, Lowering the band gap of anatase-structured TiO_2 by coalloying with Nb and N: electronic structure and photocatalytic degradation of pethylene blue dye, J. Phys. Chem. C 116 (2012) 5986–5994.
[9] J. Nowotny, T. Norby, T. Bak, Reactivity between titanium dioxide and water at elevated temperatures, J. Phys. Chem. C 114 (2010) 18215–18221.
[10] K.W. Park, K.S. Seol, Nb–TiO_2 supported Pt cathode catalyst for polymer electrolyte membrane fuel cells, Electrochem. Commun. 9 (2007) 2256–2260.
[11] R. Asahi, et al., Visible-light photocatalysis in nitrogen-doped titanium oxides, Science 293 (2001) 269–271.
[12] S. Soni, M.J. Henderson, J.F. Bardeau, A. Gibaud, Visible-light photocatalysis in titania based mesoporous thin films, Adv. Mater. 20 (2008) 1493–1498.
[13] T.L. Hsiung, H.P. Wang, H.C. Wang, XANES studies of photocatalytic active species in nano TiO_2–SiO_2, Radiat. Phys. Chem. 7 (2006) 2042–2045.
[14] R. Fuentes, B.L. Garcia, J.W. Weidner, Effect of titanium dioxide supports on the activity of Pt–Ru toward electrochemical oxidation of methanol, J. Electrochem. Soc. 158 (5) (2011) 461–466.
[15] B. Mei, et al., The synthesis of Nb-doped TiO_2 nanoparticles by spray drying: an efficient and scalable method, J. Mater. Chem. 21 (2011) 11781–11790.
[16] J. Yang, et al., Solar photocatalytic activities of porous Nb-doped TiO_2 microspheres prepared by ultrasonic spray-pyrolysis, Solid State Sci. 14 (2012) 139–144.
[17] N.R. Elezovic, B.M. Babic, L. Gajic-Krstajic, V. Radmilovic, N.V. Krstajic, L.J. Vracar, Synthesis, characterization and electrocatalytical behavior of Nb–TiO_2/Pt nanocatalyst for oxygen reduction reaction, J. Power Source 195 (2010) 3961–3968.
[18] J. Arbiol, J. Gerda, G. Dezanneau, A. Cirera, F. Peiro, Effects of Nb doping on the TiO_2 anatase to rutile phase transition, J. Appl. Phys. 92 (2002) 853–861.
[19] D.A. Shirley, High-resolution X-ray photoemission spectrum of the valence bands of gold, Phys. Rev. B 5 (1972) 4707–4709.
[20] D.J. Kim, S.H. Hahn, S.H. Oh, E.J. Kim, Influence of calcination temperature on structural and optical properties of TiO_2 thin films prepared by sol–gel dip coating, Mater. Lett. 57 (2002) 355–360.
[21] B.L. Kirsch, E.K. Richman, A.E. Riley, S.H. Tolbert, In-situ X-ray diffraction study of the crystallization kinetics of mesoporous titania films, J. Phys. Chem. B 108 (2004) 12698–12700.
[22] J.H. Park, S.J. Kang, S.I. Na, Indium-free, acid-resistant anatase Nb doped TiO_2 electrodes activated by rapid-thermal annealing for cost-effective organic photovoltaics, Sol. Energy Mater. Sol. Cell 95 (2011) 2178–2185.
[23] M.C. Biesinger, L.W.M. Lau, A.R. Gerson, R.S.T. Smart, Resolving surface chemical states in XPS analysis of first row transition metals, oxides and hydroxides: Sc, Ti, V, Cu and Zn, Appl. Surf. Sci. 257 (2010) 887–898.
[24] J. Yu, X. Zhao, Q. Zhao, Photocatalytic activity of nanometer TiO_2 thin films prepared by the sol–gel method, Mater. Chem. Phys. 69 (2001) 25–29.
[25] J. Pouilleau, D. Devilliers, H. Groult, P. Marcus, Surface study of a titanium-based ceramic electrode material by X-ray photoelectron spectroscopy, J. Mater. Sci. 32 (1997) 5645–5651.
[26] S.M. Kumbar, G.V. Shanbhag, F. Lefebvre, S.B. Halligudi, Heteropoly acid supported on titania as solid acid catalyst in alkylation of *p*-cresol with *tert*-butanol, J. Mol. Catal. A: Chem. 256 (2006) 324–334.
[27] C.D. Wagner, W.M. Riggs, L.E. Davis, J.F. Moulder, G.E. Muilenberg, Handbook of X-ray Photoelectron Spectroscopy, PerkinElmer corporation, USA, 1979.
[28] C. Massaro, P. Rotolo, F. De Riccardis, E. Milella, Comparative investigation of the surface properties of commercial titanium dental implants. Part I: Chemical composition, J. Mater. Sci.: Mater. Med. 13 (2002) 535–548.
[29] Z.D. Mitrovic, Z.V. Popovic, M. Scepanovic, Anharmonicity effects in nanocrystals studied by Raman scattering spectroscopy, Acta Phys. Pol. A 116 (2009) 36–41.
[30] M.J. Šćepanović, M.G. Brojčin, Z.D. Mitrović, Z.V. Popović, Characterization of anatase TiO_2 nanopowder by variable-temperature Raman spectroscopy, Sci. Sinter. 41 (2009) 67–73.
[31] M.S. Chebil, G. Vignaud, Y. Grohens, O. Konovalov, M.K. Sanyal, T. Beuvier, A. Gibaud, In situ X-ray reflectivity study of polystyrene ultrathin films swollen in carbon dioxide, Macromolecules 45 (2012) 6611–6617.
[32] R.C. Suciu, E. Indrea, T.D. Silipas, TiO_2 thin films prepared by sol–gel method, J. Phys. Conf. Series 182 (2009) 12080.
[33] A. Rahdar, V. Arbabi, H. Ghanbari, Study of electro-optical properties of ZnS nanoparticles prepared by colloidal particles method, Int. J. Chem. Biol. Eng. 6 (2012) 81–83.
[34] A.E.J. Gonzalez, S.G. Santiago, Structural and optoelectronic characterization of TiO_2films prepared using the sol–gel technique, Semicond. Sci. Technol. 22 (2007) 709–716.